

Gas monitoring in human sinuses using tunable diode laser spectroscopy

Linda Persson
Mats Andersson
Märta Cassel-Engquist
Lund University
Division of Atomic Physics
P.O. Box 118
SE-221 00 Lund, Sweden

Katarina Svanberg
Lund University Hospital
Department of Oncology
SE-221 85 Lund, Sweden

Sune Svanberg
Lund University
Division of Atomic Physics
P.O. Box 118
SE-221 00 Lund, Sweden

Abstract. We demonstrate a novel noninvasive technique based on tunable diode laser absorption spectroscopy to investigate human sinuses *in vivo*. The technique relies on the fact that free gases have spectral imprints that are about 10,000 times sharper than spectral structures of the surrounding tissue. Two gases are detected; molecular oxygen at 760 nm and water vapor at 935 nm. Light is launched fiber optically into the tissue in close proximity to the particular maxillary sinus under study. When investigating the frontal sinuses, the fiber is positioned onto the caudal part of the frontal bone. Multiply scattered light in both cases is detected externally by a handheld probe. Molecular oxygen is detected in the maxillary sinuses on 11 volunteers, of which one had constantly recurring sinus problems. Significant oxygen absorption imprint differences can be observed between different volunteers and also left-right asymmetries. Water vapor can also be detected, and by normalizing the oxygen signal on the water vapor signal, the sinus oxygen concentration can be assessed. Gas exchange between the sinuses and the nasal cavity is also successfully demonstrated by flushing nitrogen through the nostril. Advantages over current ventilation assessment methods using ionizing radiation are pointed out. © 2007 Society of Photo-Optical Instrumentation Engineers. [DOI: 10.1117/1.2777189]

Keywords: infrared spectroscopy; diode lasers; molecular spectroscopy; medicine; scattering.

Paper 07111R received Mar. 23, 2007; revised manuscript received Jun. 11, 2007; accepted for publication Jun. 11, 2007; published online Sep. 12, 2007.

1 Introduction

The human paranasal sinuses are air-filled cavities embedded in the cranial skeleton. The frontal sinuses are located behind the frontal bone, while the maxillary sinuses are located below the orbital floor in the cheek bones. The sphenoidal sinus, split by a partial wall, is located centrally in the cranium. The ethmoidal cells are multifocal small cavities located on each side of the upper part of the nose cavity. The sinuses are lined with epithelium-bearing glands and cilia, which transport mucosa toward the channel, or ostium, connecting the sinus to the nasal cavity. The frontal and maxillary sinus ostia connect to the middle nasal meatus. The function of sinuses is still under discussion. They seem to be locations of nitric oxide production important for ventilation functions.^{1,2} The anatomy of the head is shown in Fig. 1(a),³ with the sinuses schematically indicated; the frontal and maxillary sinuses are clearly discerned in the magnetic resonance image (MRI) shown in Fig. 1(b).

Good ventilation seems to be a requisite for healthy sinuses. Infection in the cavities, sinusitis, is affecting a very large number of patients, in the U.S. alone about 37 million people are annually diagnosed.⁴ Narrow ostia or partial or full blockage can cause severe problems and chronic sinusitis. Na-

sal polyps can be one cause. Excessive mucosal and pus production are secondary signs of sinusitis. Infection is frequently treated with antibiotics, and decongestants, such as oxymetazoline and zylometazoline, are prescribed to improve ventilation. Surgical intervention with intended ostial widening is necessary in severe cases for achieving long-term improvement. Clearly, a precise diagnosis of sinusitis is of importance, particularly for deciding whether antibiotics should be administered or not. Common present diagnostics may include the use of ultrasound, capable of seeing from the echo structure if the cavity is air filled or not, and in severe cases the use of x-ray radiography. However, none of these techniques can assess the ventilation of the cavities or the composition of enclosed gas.

Ventilation studies for the paranasal sinuses have been pursued with intrusive and noninvasive techniques. Among the former, cannulae have been used to measure pressure in the sinuses and in the nasal cavity and their interrelation. Nitrogen gas has also been injected as well as gaseous radioactive isotopes, in particular Xe¹³³, with a half-life of 5.2 days. Scintillation cameras or single photon emission computerized tomography (SPECT) have been used to assess the transport of the gas. Xe¹³³ has also been administered noninvasively through breathing, followed by repeatedly performing the Valsalva maneuver.⁵ Stable Xe gas, having a certain radio opac-

Address all correspondence to: Linda Persson, Atomic Physics Division, Department of Physics, Lund University - P.O. Box 118, Lund, Skåne 221 00 Sweden; Tel: +46 46 2224138; Fax: +46 46 222 42 50; E-mail: linda.persson@fysik.lth.se

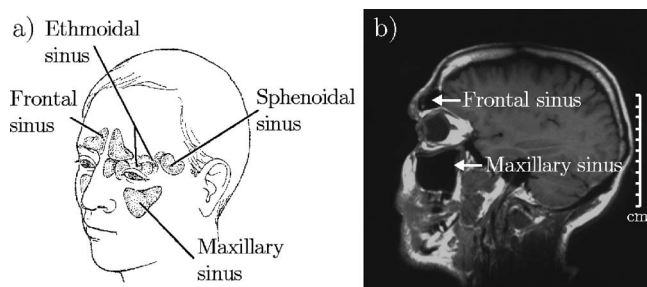


Fig. 1 (a) Illustration showing the location of the human sinuses (adopted from Ref. 3). (b) MRI image indicating the location of human maxillary and frontal sinuses.

ity, has also been used noninvasively, followed by repeated computerized tomographic (CT) recordings.⁶ Clearly, these methods expose the patients to a considerable radiological dose. Further, radioactive as well as stable Xe gas is very costly, as is the use of SPECT and CT installations. Hyperpolarized ³He has been used in MRI studies,⁷ also costly investigations. Thus, there is a need for a complementary technique avoiding these hazards and costs while still allowing a detailed assessment of ventilation and gas composition.

We demonstrate the possibility to statically and dynamically noninvasively study human sinuses by observing the normal physiological gases of oxygen and water vapor. This is done by using tunable diode laser spectroscopy on the gases exhibiting narrow-band absorptive imprints in the near infrared spectral region. The present study extends and establishes the methodology, which was first described in two recent exploratory papers.^{8,9}

The new development became possible by taking advantage of optical spectroscopic techniques refined in the environmental monitoring of free gas, and an understanding of tissue optics, developed for purposes such as optical mammography and photodynamic therapy dosimetry (e.g., Ref. 10). We could thus demonstrate the possibility to investigate the frontal sinuses using tunable diode laser spectroscopy employing phase sensitive detection of wavelength-modulated absorption signals.⁸ The presence of molecular oxygen was measured close to 760 nm in a backscattering detection geometry. To understand the behavior of the expected signals, a phantom was first investigated. It consisted of two Delrin plates separated by a variable air gap, where the first plate represented the frontal bone, the air space the frontal sinus, and the second plate the underlying tissue. Some preliminary results from a human frontal sinus were obtained. These measurements have been modeled in Monte Carlo simulations, and the possibility of imaging using a scanned probe was discussed.¹¹ Since then, the experimental techniques have been improved by using pigtailed lasers and balanced detection to suppress noise.¹² This allowed us to study gas exchange between the maxillary sinuses and the nasal cavity by using a transmission detection geometry. The fiber was placed inside the mouth on the palate and the detector externally on the cheek bone. For a short time, the nasal cavity was flushed through the nostril with nitrogen gas and the decay of the oxygen signal was recorded on a healthy volunteer, resulting in the conclusion that the channels between the cavities were open, allowing free gas exchange. No such behavior could be

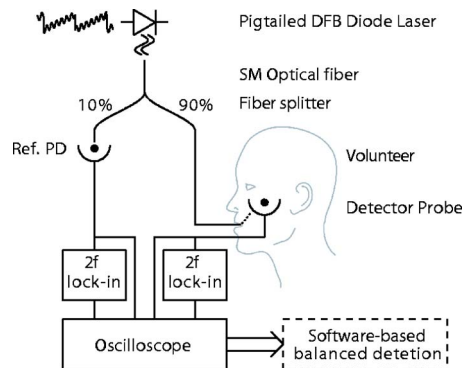


Fig. 2 Schematic drawing of the experimental setup used to study human sinuses.

observed on a volunteer with constantly recurring sinus problems.⁹

We demonstrate molecular oxygen measurements on maxillary sinuses for 11 healthy volunteers using the transmission detection geometry discussed. The measured values have been compared with values obtained using Monte Carlo simulations of a model representing the maxillary sinuses. To further investigate the clinical potential of the technique, other different possible detection geometries have been explored, allowing monitoring of both the maxillary and the frontal sinuses. A further gas—water vapor interrogated at 935 nm—has also been studied, providing new information. Water vapor lines around 980 nm were studied in a previous paper on drying processes.¹³ Since liquid water, always abundantly present in human tissue, also has an absorption peak at 980 nm, we now choose a shorter wavelength where most of the liquid water absorption is eliminated to allow depth penetration. Investigations of the gas exchange of the sinuses and the nasal cavity in the different geometries have as well been performed using pure nitrogen gas flushed through the nostril.

In the next section, the experimental setup and the data analysis are presented. The gas monitoring procedure, including the different detection geometries used, are described, followed by an explanation of the model used in the Monte Carlo simulations. Results of the measurements of the maxillary and frontal sinuses using the different detection geometries are then presented and discussed. Finally, conclusions are drawn and suggestions for further work are put forward.

2 Materials and Methods

2.1 Experimental Setup

A schematic drawing of the experimental setup used in this study is shown in Fig. 2. In the case of molecular oxygen detection, a single-mode pigtailed distributed feedback (DFB) diode laser (Nanoplus, Germany) operating at around 760 nm with an output of about 4 mW is used as a spectroscopic light source. When performing measurements on water vapor, the laser is changed to another unit operating around 935 nm (Nanoplus, Germany) with similar output. The laser is scanned across an absorption line of the gas under study by supplying a saw-tooth ramp (Hz) to the laser driver current. To achieve wavelength modulation spectroscopy (WMS) with lock-in detection, the operating current is also modulated by a

sinusoidal wave at 9 kHz, with a modulation index of about 2.2 in both gas cases. In the case of molecular oxygen, the R11Q12 absorption line at 760.445 nm (vacuum wavelength) is used, and in the case of water vapor, the absorption line at 935.686 nm (vacuum wavelength) is used [vibration; (000) \rightarrow (121), rotation; $J''=3 \rightarrow J'=4$, $K''_a=0 \rightarrow K'_a=0$, $K''_c=3 \rightarrow K'_c=4$].

The light is fiber optically split 90/10(%) into two parts with a single-mode fiber-coupled beamsplitter (Laser2000, Sweden). The low-intensity part is directly guided to a silicon detector (UDT 10DP/SB). This part is later used in the analysis as the reference beam to obtain balanced detection for efficient noise subtraction.¹² The other part is guided to different positions on the human head, and the multiply scattered light is detected externally on the human head according to different detection geometries further discussed in Sec. 2.3 on the *gas monitoring procedure*. In the case of molecular oxygen detection, a photomultiplier tube (PMT) (Hamamatsu 5070A) with a circular detection area of 20 mm diam is used, and in the case of water vapor detection, a photodiode (Hamamatsu S3584-06) with similar detection area is used. Both detectors are mounted as handheld probes.

The two detected signals are each divided into two parts. They are sent to a computer-controlled digital oscilloscope, one directly, referred to as the direct signal, and one via a lock-in amplifier where the signal at twice the modulation frequency is recorded, referred to as the $2f$ signal. WMS is often referred to as derivative spectroscopy, since the different harmonics are proportional to the corresponding derivative of the signal. Thus, in the case of detection at twice the modulation frequency, the $2f$ signal looks like the second derivative of the direct absorption.

2.2 Data Analysis

The $2f$ signals are normalized with the direct signals to make them independent of the amount of light reaching the detector. The normalized $2f$ sample signal is then subtracted with a processed version of the reference signal to achieve a balanced detection signal.¹² An ideal absorption signal is then fitted to the balanced detection signal, and from this the peak-to-peak distance is estimated, referred to as the WMS value. For small absorptions, the WMS value is proportional to the absorbance, and thus to the product of the gas concentration and the path length traveled by the light. To transform the WMS value to a more meaningful quantity, the standard addition method is used.¹⁴ The standard addition procedure is to add known path lengths of ambient air in-between the light source and the detector. At each distance, the WMS value is measured. A so-called equivalent mean path length L_{eq} can then be estimated, corresponding to the air distance that the light has to travel in ambient air to obtain the same oxygen or water vapor absorption imprint. The calibration procedures for both gases were performed at room temperature of 25°C and a relative humidity of about 20%. It should be noted that one would expect 100% humidity in the sinus cavities due to liquid water in the surrounding tissue, with a temperature close to 37°C. At such a temperature, the water vapor pressure is about a factor of 2 higher than at 25°C.¹⁵ Thus, a particular water vapor signal from a sinus corresponds to about 1/10 of the surrounding air path length yielding the

same signal. This factor is further discussed in Sec. 4.

2.3 Gas Monitoring Procedure

The maxillary and frontal sinuses of human volunteers were investigated using the noninvasive technique presented. In the case of the maxillary sinus, two different detection geometries were used (*PC* and *CC*), and in the case of frontal sinus studies, a single detection geometry was used (*OF*) as follows.

- (*PC*) *Palate - cheek bone geometry*: fiber placed inside the mouth against the palate close to the sinus under study and the detector positioned on and around the cheek bone.

- (*CC*) *Cheek - cheek bone geometry*: fiber placed outside on the cheek below the cheek bone and the detector positioned on the cheek bone.

- (*OF*) *Orbital edge - frontal bone geometry*: fiber placed on the horizontal part of the frontal bone under the eyebrow pointing up toward the frontal bone and the detector placed at different positions on the frontal bone.

Before any measurements were performed on any human sinuses, two types of reference measurements were carried out to investigate any possible L_{eq} offset in the current setup. The oxygen and water vapor signal were measured through the cheek below the cheekbone and through the hand of the volunteers where no free gas is expected. These measurements resulted in a consistently nondetectable gas imprint signal, showing that no gas offset is present due to gas between the setup components.

Molecular oxygen measurements were performed with geometry *PC* on 11 volunteers, 10 of which have no history of sinus problems (volunteers 1 to 10) and one with constantly recurring sinus problems (volunteer 11). The detector was placed at three different positions; on the cheek bone, slightly toward the nose, and slightly under the cheek bone. At each detector position, three consecutive measurements were performed by removing and repositioning the fiber and the detector between each recording. The reproducibility of the measured L_{eq} values was also investigated by measuring ten consecutive times at each detector position for one volunteer.

Measurements of oxygen and water vapor were performed with detection geometry *PC* on the maxillary sinuses on volunteers 1, 2, and 11, and on volunteer 1 also with geometry *CC*. In addition, frontal sinus measurements with geometry *OF* were performed on volunteer 1. In the case of geometry *PC* and *CC*, the detector was positioned on the cheek bone. In the case of frontal sinus study, detection geometry *OF*, the detector was positioned at three different locations on the frontal bone toward the particular sinus; about 10 mm and about 20 mm straight up above the light source, and about 10 mm straight up over the center of the eyebrow. At each detector position, ten consecutive measurements were performed by removing the fiber and the detector between each recording. Molecular oxygen was measured first, followed by water vapor directly after using the same procedure.

To study the communication and ventilation between the nasal cavity and the human sinuses, we investigated the transient response to pure nitrogen flushing of the nasal cavity for about 1 min through the nostril. These measurements were performed on volunteer 1 with all detection geometries and volunteer 11 with detection geometry *PC*. Measurements were continuously recorded for about 8 min. 1 min before

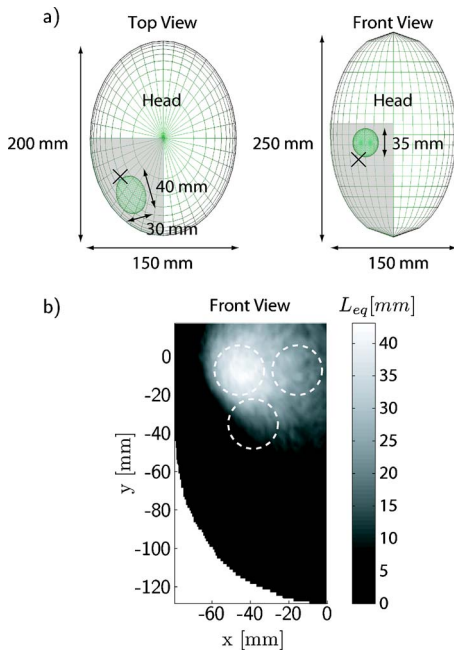


Fig. 3 (a) A model used for Monte Carlo simulations created in ASAP™ representing measurements on the human maxillary sinus according to detector geometry *PC*. The region where the rays were collected is indicated by the gray shaded area. The cross represents the location of the light source. (b) The simulated L_{eq} for the model shown in (a). The different positions of the detector in the case of real measurements are also indicated.

flushing, 1 min during flushing, and 6 min after terminating the flush, all the time pursuing normal mouth breathing. Each recorded signal was averaged for about 15 sec. Measurements of molecular oxygen and water vapor were performed directly after each other. To investigate the stability of the recorded signals for the gas exchange study time period, the same procedure was also carried out without N₂ flush.

2.4 Simulations

Monte Carlo simulations were performed by using the Advanced Systems Analysis Program (ASAP) software.¹⁶ In this work, we present a model according to Fig. 3(a) to simulate measurements on the maxillary sinuses employing detection geometry *PC* when detecting the multiply scattered light on and around the cheek bone. The position of the light source is indicated by a cross in the model. The maxillary sinus was

represented by an ellipsoid with typical human dimensions. It was placed embedded in a scattering medium with optical properties set to $g=0.87$ (anisotropy factor), $\mu_s=16 \text{ mm}^{-1}$ (scattering coefficient), and $\mu_a=0.0005 \text{ mm}^{-1}$ (absorption coefficient) typical of bone.¹⁷

The flux and the pattern through the model for rays reaching the detector were recorded. The distance each ray traveled in the ellipsoid was calculated. By summarizing the product of the distance in the cavity and the flux for each ray and normalizing it with the total flux reaching the detector, the L_{eq} value could be estimated. Similar simulations have been presented in Ref. 11 for frontal sinus imaging.

3 Results and Discussion

3.1 Maxillary Sinus Study

Figure 3(b) shows L_{eq} obtained through simulation measurements on the maxillary sinuses according to detection geometry *PC*. It can be seen that L_{eq} values between 10 and 40 mm can be expected when performing measurements on volunteers with typical maxillary sinus dimensions when the detector is placed on and around the cheek bone. These values are heavily influenced by the optical properties used in the simulations, but can still be used as an indication of the experimental results to be expected. If, for example, a higher absorption coefficient is used, as was experimentally obtained by Hoshi et al.,¹⁸ a decrease of L_{eq} would be obtained.

The results from the molecular oxygen measurements on the volunteers according to geometry *PC* are presented in Table 1. The L_{eq} value shown is an average from the three different detector positions. It was observed that the lowest L_{eq} is always recorded when the detector is positioned below the cheek bone, in agreement with the simulation results, where the detection areas are also indicated [Fig. 3(b)]. All volunteers with no history of sinus problems presented a detectable oxygen absorption imprint. However, no oxygen imprint could be recorded on the left side of volunteer 11. The reproducibility of the measured L_{eq} values was also investigated at each detector position for one volunteer. A standard deviation of about 10% was obtained when the average measured L_{eq} value was of the order of 30 mm. A clear left-right asymmetry was observed for volunteer 11 as discussed before. Smaller asymmetries were observed also for other volunteers. However, it should be noted that the L_{eq} value depends on concentration as well as path length, and thus detailed analysis regarding anatomy are hard to draw.

The results from the measurements of oxygen and water

Table 1 Measured L_{eq} values for oxygen in the maxillary sinus for volunteers 1 through 11 according to detection geometry *PC*. N represents volunteers with no history of sinus problems and Y the volunteer with constantly recurring sinus problems. The presented values are averaged from three different detector positions; on the cheek bone, slightly toward the nose, and slightly under the cheek bone.

Volunteer history	1	2	3	4	5	6	7	8	9	10	11
	N	N	N	N	N	N	N	N	N	N	Y
Left L_{eq} [mm]	20±4	29±6	8±7	24±3	18±2	12±9	25±0	13±9	28±0	11±2	-
Right L_{eq} [mm]	27±7	31±3	17±2	16±4	21±8	13±6	23±1	12±6	29±9	12±2	10±3

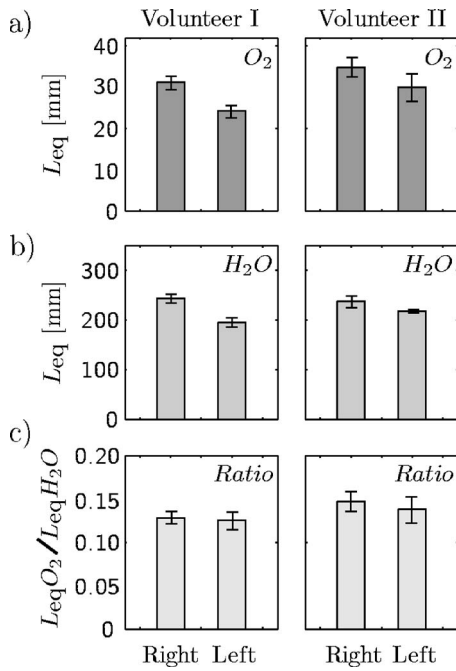


Fig. 4 L_{eq} for (a) molecular oxygen and (b) water vapor measured in left and right maxillary sinuses for volunteers 1 and 2 using detection geometry PC with the detector positioned on the cheek bone. The data shown correspond to the average of ten recordings together with two standard deviations. (c) The ratios of the L_{eq} for oxygen and water vapor are shown.

vapor with detection geometry PC on the maxillary sinuses on volunteers 1 and 2 are shown in Figs. 4(a) and 4(b). The average L_{eq} values are presented together with two standard deviations. It should be noted that the recorded L_{eq} for water vapor is about 8 larger than the value for oxygen for volunteers 1 and 2. The same types of measurements were attempted on volunteer 11. An oxygen signal of $L_{eq}=13$ mm was detected for the right sinus, whereas no signal could be observed for the left side. No water vapor signal could be detected on the right side due to heavy overall absorption in the tissue and the partially filled sinus cavity.

As discussed previously, the estimated L_{eq} depends on both the concentration of the gas and the scattering properties of the tissue. It can be assumed that the scattering properties are approximately the same for the two different wavelengths used.^{19,20} However, the absorption coefficient may be different mostly depending on the degree of oxygenation of the blood and liquid water absorption.^{17,19} If the same volume has been sampled for the two wavelengths, the ratio between the L_{eq} values for oxygen and water vapor could provide information on the oxygen concentration inside the sinuses, since the water vapor concentration is always the maximum possible concentration at the given temperature (thermostated to about 37°C and 100% humidity in the cavities). In Fig. 4(c), the ratios for the left and right maxillary sinus are shown. On volunteers 1 and 2, it can be seen that this ratio is about the same for both sides. It can also be seen that the two volunteers maintain similar ratios. The average ratio is 0.13 ± 0.01 . Assuming that these volunteers have healthy and well ventilated sinuses with about 20% oxygen concentration, a reduced ratio

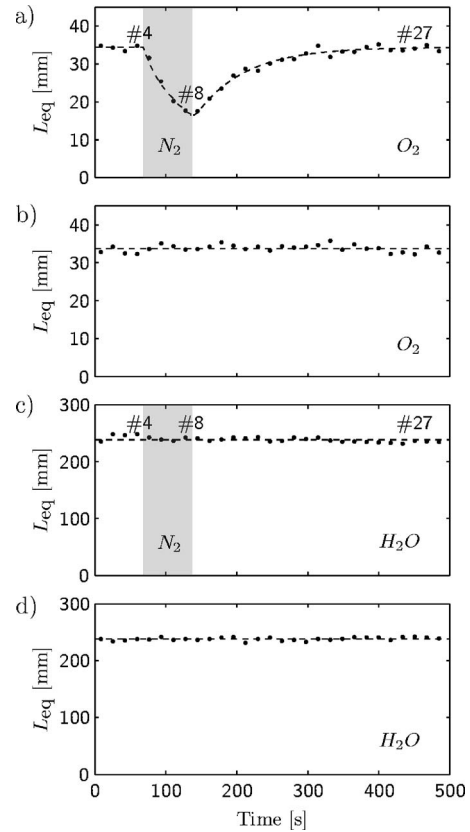


Fig. 5 Gas exchange study for the right maxillary sinuses using detection geometry PC on volunteer 1 (see text). (a) L_{eq} for oxygen (solid dots) measured as a function of time with N_2 flushing, together with a line drawn for guidance of the eye (dashed line). (b) Same as (a) without N_2 flushing. (c) L_{eq} for water vapor (solid dots) measured as a function of time with N_2 flushing. (d) same as (c) without N_2 flushing.

may indicate a lower oxygen concentration in the cavity.

Gas exchange studies were performed on volunteers 1 and 11 with the same detection geometry PC. A reduction of the oxygen absorption imprint could be observed on volunteer 1 when flushing with N_2 , as well as the reperfusion of air when terminating the N_2 flush [Fig. 5(a)]. In Fig. 5(b), the stability of the oxygen signal during the same time scale without N_2 flush can be seen. In the case of water vapor detection, no reduction of the signal could be recorded during N_2 flush [Fig. 5(c)]. A series of water vapor signal measurements is also shown in Fig. 5(d), illustrating the stability of the data. The results indicate that the flushing is not able to change the humidity in the cavities. Figure 6 shows signals recorded at three different time intervals during the gas exchange study (indicated by corresponding numbers in Fig. 5). The fractional absorption was 8.6×10^{-4} and 6.7×10^{-3} for the largest signals observed for oxygen and water vapor, respectively. The signals from reference measurements through the cheek directly after the study are also shown. The same molecular oxygen measurements with nitrogen flushing were performed on the right maxillary sinus of volunteer 11. These measurements did not show any decrease in oxygen signal during the N_2 flush period, indicating lack of communication with the nasal cavity.

Oxygen and water vapor were measured according to ge-

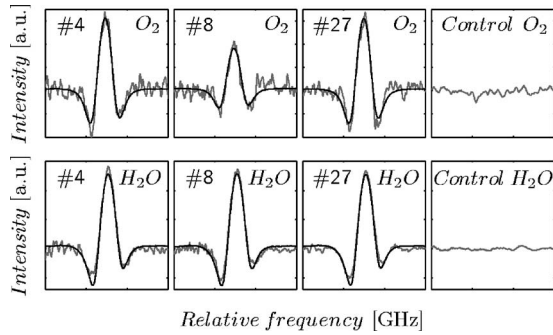


Fig. 6 Balanced detection signals measured for oxygen and water vapor during the gas exchange study using detection geometry *PC*. The numbers correspond to the ones indicated in Fig. 5. The relative frequency range is about 30 GHz. The control signals are also shown for both gases when measuring through the cheek.

ometry *CC* on the maxillary sinuses of volunteer 1 [see Figs. 7(a) and 7(b)]. We note a left-right asymmetry stronger than observed for the same volunteer with data shown in Fig. 4 (left) when using a different detection geometry. This indicates that tomographic information might be extracted regarding anatomy using multiple geometries. The ratio between the signals is shown for both sides in Fig. 7(c). An average ratio of 0.12 ± 0.01 is obtained for this geometry.

The same gas exchange procedure was carried out with detection geometry *CC* on volunteer 1 (see Fig. 8). The same behavior was observed as for detection geometry *PC*.

3.2 Frontal Sinus Study

Measurements of the frontal sinuses were performed on volunteer 1 with detection geometry *OF*. In Figs. 9(a) and 9(b), the average L_{eq} together with two standard deviations is shown for the two gases, and the three different detector positions discussed above and seen in the top of Fig. 9. The ratio between the L_{eq} for oxygen and water vapor can be seen in Fig. 9(c). An average of 0.12 ± 0.01 is obtained.

The gas exchange between the nasal cavity and the frontal sinuses was also studied with geometry *OF*. In Fig. 10, the invasion of N_2 and reinvasion of ambient air can be seen for volunteer 1 when detecting oxygen. Again, no such phenomena could be observed when detecting water vapor.

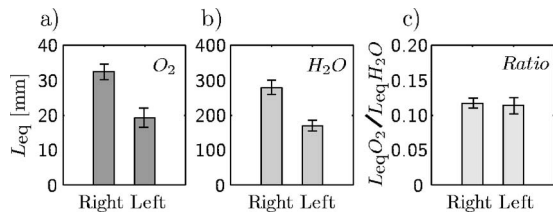


Fig. 7 L_{eq} for (a) molecular oxygen and (b) water vapor measured in left and right maxillary sinuses for volunteer 1 using detection geometry *CC*. The data shown correspond to the average of ten recordings together with two standard deviations. (c) The ratios of the L_{eq} for oxygen and water vapor are shown.

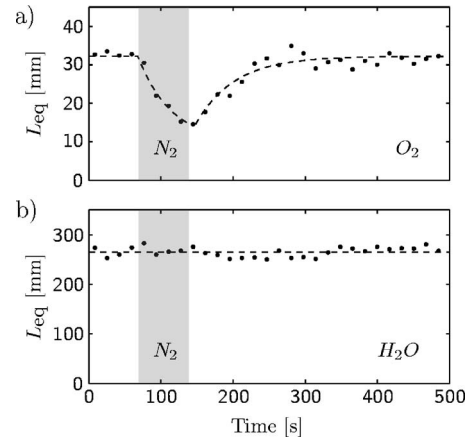


Fig. 8 Gas exchange study for the maxillary sinuses using detection geometry *CC* on volunteer 1 (see text). (a) L_{eq} for oxygen (solid dots) measured as a function of time with N_2 flushing, together with a line drawn for guidance of the eye (dashed line). (b) L_{eq} for water vapor (solid dots) measured as a function of time with N_2 flushing.

4 Conclusion and Outlook

We show that nonintrusive diode laser spectroscopy with monitoring of common physiological gases such as oxygen and water vapor is capable to assess important aspects of hu-

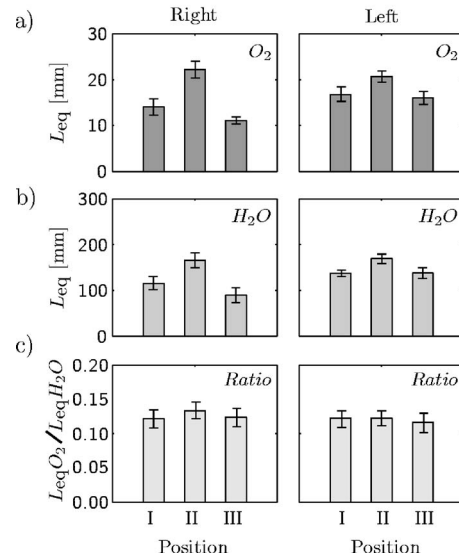
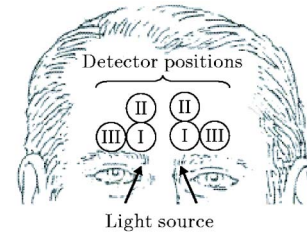


Fig. 9 L_{eq} for (a) molecular oxygen and (b) water vapor measured in left and right frontal sinuses for volunteer 1 using detection geometry *OF* and detector positions according to the top figure. The data shown correspond to the average of ten recordings together with two standard deviations. (c) The ratios of the L_{eq} for oxygen and water vapor are shown.

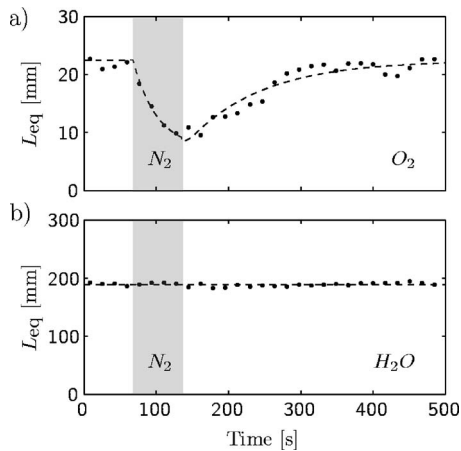


Fig. 10 Gas exchange study for the frontal sinuses using detection geometry *OF* on volunteer 1 (see text). (a) L_{eq} for oxygen (solid dots) measured as a function of time with N_2 flushing, together with a line drawn for guidance of the eye (dashed line). (b) L_{eq} for water vapor (solid dots) measured as a function of time with N_2 flushing.

man sinuses and their potential diseases. It is demonstrated that oxygen as well as water vapor can be detected within the maxillary and frontal sinuses on volunteers by employing different detection geometries discussed in Sec. 2. Individual variations and left-right asymmetries are observed. The oxygen absorption imprint levels detected are in good agreement with the results from Monte Carlo simulations implemented with ASAPTM software. By forming the ratio between the two signals (normalizing the oxygen signal on the water vapor signal), it is shown that basically the same value is obtained for all well ventilated sinuses studied. This is to be expected if a constant concentration of (about 20%) oxygen is assumed in the healthy sinuses, and if 100% water vapor saturation develops in the sinus. Further, a prerequisite would also be that the scattering and absorption coefficients are the same at 760 and 935 nm, resulting in the same effective path length through the gas-filled cavity. Consulting the literature, it can be found that this assumption is not fully warranted.^{17,19,20} In particular, the absorption coefficient depends on the degree of blood oxygenation and amount of liquid water, and would tend to increase the absorption at 935 nm, as compared to 760 nm. The scattering coefficient could be expected to be the same within about 10%. The fact that a very similar signal ratio is obtained for different volunteers, sinuses and geometries, suggests that the assumption of a similar effective path length is reasonable. We notice, however, that the experimental ratio was found to be about 0.12. Going from 20% relative humidity to 100% influences the equivalent mean path length by a factor of 5. Likewise, going from 25 to 37°C introduces a factor of 2 in water potential pressure.¹⁵ Thus an experimental ratio of 0.10 would be expected. The measured value of 0.12 could thus be interpreted in two ways. The air is not attaining 37°C in dynamic exchange but only about 33°C, which is not unlikely. A further explanation is that the effective sample pathway for the two wavelengths differ by a factor of 1.2 with a smaller path length at 935 nm due to increased absorption. A combination of the two effects could be present. Given that the experimentally observed effects are

rather small, it seems like it should be possible to perform an empirical correction after having gained clinical data. The results of the present work would mean that it would be possible to noninvasively read off the oxygen concentration in a sealed-off sinus cavity, which might be of clinical value if a correlation to pathology could be established in a clinical trial. It should be noted that a water vapor signal is always expected as soon as there is a gas-filled cavity. A zero reading for oxygen would then by necessity mean that no oxygen is present in the gas, not that the cavity contains no gas at all.

We also demonstrate that the ventilation of the sinuses (the ostial function) could easily be measured observing the oxygen signal, which is reduced when nitrogen gas is given through the nostril as a displacement gas while the patient is breathing normally through the mouth. By instead administering high-concentration oxygen gas, a much stronger signal can favorably be achieved. The time constants for the gas exchange can be determined by fitting the curves. The convenience of a combination of a physiological gas and light for gas exchange studies is in strong contrast to the previous use of stable or radioactive xenon gas in combination with repeated CT scans or SPECT imaging, both leaving the patient with a considerable dose of ionizing radiation. It was found that the concentration of water vapor in the sinuses was not influenced by the flushing with dry nitrogen gas. The conclusion is that 100% water saturated gas is immediately obtained in the sinus. This fact also corroborates the earlier finding that water vapor reliably can be used as a reference gas of known concentration in the well thermostated sinus (at 33 to 37°C). By recording the relative intensity of two suitable oxygen or water vapor lines, and their half-width with sufficient precision, the temperature and pressure can in principle be measured.

Sequential measurements are made on oxygen and water vapor in the present studies. In a clinically adapted system, the two types of measurements could in principle be made simultaneously using the same detector and different modulation frequencies. When exactly the same geometry pertains for both kinds of measurements an even better stability for the ratio signal can be expected. A clinical trial on sinus patients jointly with an ear-nose-throat (ENT) clinic is planned to assess the clinical practicality and potential benefits of the new technique.

The demonstrated possibility to noninvasively assess the oxygen concentration in a hollow organ by sending light through a substantial layer of human tissue suggests that the new technique might have important applications in assessing the lung function in newborn and small children. With higher power lasers, still without any noticeable thermal effect, corresponding measurements on the lung lobes in adults should be feasible in lung ventilation studies, where, however, the empirical path length difference correction might be larger.

Acknowledgments

The authors are grateful for fruitful discussions with N. G. Holmer, M. Jannert, K. Jonsson, L. Malm, and K. Prellner. We are grateful to L. Simonsson and E. Kristensson for collaboration on ASAPTM simulations. This research was supported by the Swedish Research Council, the Medical Faculty at Lund University, and the Knut and Alice Wallenberg Foundation.

References

1. P. Stierna, G. Karlsson, I. Melén, and M. Jannert, "Aspect on sinusitis—diagnosis and treatment in adults," *Proc. Mtg. Swedish Assoc. Otorhinolaryngol.*, pp. 7–30, HNS, Stockholm (1995).
2. T. Runer and S. Lindberg, "Effects on nitric oxide on blood flow and mucociliary activity in the human nose," *Ann. Otol. Rhinol. Laryngol.* **107**, 40–46 (1998).
3. See <http://cfcenter.stanford.edu/CFNews-Sinusitis.html>.
4. *Health Matters, Sinusitis*, Nat. Inst. Allergy and Infectious Diseases, U.S. Dept. of Health and Human Services, Bethesda, MD (2005).
5. B. Paulsson, J. Dolata, I. Larsson, P. Ohlin, and S. Lindberg, "Paranasal sinus ventilation in healthy subjects and in patients with sinus disease evaluated with the 133-Xenon washout technique," *Ann. Otol. Rhinol. Laryngol.* **110**, 667–674 (2001).
6. D. Leopold, S. J. Zinreich, B. A. Simon, M. M. Cullen, and C. Marcucci, "Xenon-enhanced computed tomography quantifies normal maxillary sinus ventilation," *Otolaryngol.-Head Neck Surg.* **122**, 422–424 (2000).
7. R. R. Rizi, I. E. Dimitrov, A. Thompson, G. Jones, T. R. Gentile, M. Ishii, R. Reddy, M. D. Schnall, and J. S. Leigh, "MRI of hyperpolarized ^3He in human paranasal sinuses," *Magn. Reson. Med.* **39**, 865–868 (1998).
8. L. Persson, K. Svanberg, and S. Svanberg, "On the potential of human sinus cavity diagnostics using diode laser gas spectroscopy," *Appl. Phys. B* **82**, 313–317 (2006).
9. L. Persson, M. Andersson, T. Svensson, M. Cassel-Engquist, K. Svanberg, and S. Svanberg, "Non-intrusive optical study of gas and its exchange in human maxillary sinuses," *Proc. SPIE* **6628**, 662804 (2007).
10. S. Svanberg, "Environmental and medical applications of photonic interactions," *Phys. Scr., T* **T110**, 39–50 (2004).
11. L. Persson, E. Kristensson, L. Simonsson, and S. Svanberg, "Monte Carlo simulations of optical human sinusitis diagnostics," *J. Biomed. Opt.* (in press).
12. L. Persson, F. Andersson, M. Andersson, and S. Svanberg, "Approach to optical interference fringes reduction in diode laser absorption spectroscopy," *Appl. Phys. B* **87**, 523–530 (2007).
13. M. Andersson, L. Persson, M. Sjöholm, and S. Svanberg, "Spectroscopic studies of wood-drying processes," *Opt. Express* **14**, 3641–3653 (2006).
14. S. Svanberg, *Atomic and Molecular Spectroscopy*, 4th ed., Springer-Verlag, Berlin (2004).
15. C. Nordling and J. Österman, *Physics Handbook*, 4th ed., Studentlitteratur, Lund (1987).
16. B. Michel and T. Beck, "Raytracing in medical applications," *Lasers Photon.* **5**, 38–41 (2005).
17. T. Vo-Dinh, *Biomedical Photonics Handbook*, CRC Press LLC, New York (2003).
18. Y. Hoshi, M. Shimada, C. Sato, and Y. Iguchi, "Reevaluation of near-infrared light propagation in the adult human head: implications for functional near-infrared spectroscopy," *J. Biomed. Opt.* **10**, 064032 (2005).
19. T. Svensson, S. Andersson-Engels, M. Einarsdottir, and K. Svanberg, "In vivo optical characterization of human prostate tissue using near-infrared time-resolved spectroscopy," *J. Biomed. Opt.* **12**, 014022 (2007).
20. C. Klinteberg, A. Pifferi, S. Andersson-Engels, R. Cubeddu, and S. Svanberg, "In vivo absorption spectroscopy of tumor sensitizers with femtosecond white light," *Appl. Opt.* **44**, 2213–2220 (2005).